

Thermal Decomposition Mechanism of Disilane

Kazumasa Yoshida,[†] Keiji Matsumoto,[†] Tatsuo Oguchi,[‡] Kenichi Tonokura,^{*,†,§} and Mitsuo Koshi[†]

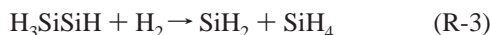
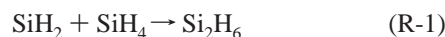
Department of Chemical System Engineering, School of Engineering, The University of Tokyo, 7-3-1 Hongo, Bunkyo-ku, Tokyo 113-8656, Japan, and Department of Ecological Engineering, Toyohashi University of Technology, Toyohashi 441-8580, Japan

Received: September 17, 2005; In Final Form: February 9, 2006

Thermal decomposition of disilane was investigated using time-of-flight (TOF) mass spectrometry coupled with vacuum ultraviolet single-photon ionization (VUV-SPI) at a temperature range of 675–740 K and total pressure of 20–40 Torr. Si_nH_m species were photoionized by VUV radiation at 10.5 eV (118 nm). Concentrations of disilane and trisilane during thermal decomposition of disilane were quantitatively measured using the VUV-SPI method. Formation of Si_2H_4 species was also examined. On the basis of pressure-dependent rate constants of disilane dissociation reported by Matsumoto et al. [*J. Phys. Chem. A* 2005, 109, 4911], kinetic simulation including gas-phase and surface reactions was performed to analyze thermal decomposition mechanisms of disilane. The branching ratio for (R1) $\text{Si}_2\text{H}_6 \rightarrow \text{SiH}_4 + \text{SiH}_2$ /(R2) $\text{Si}_2\text{H}_6 \rightarrow \text{H}_2 + \text{H}_3\text{SiSiH}$ was derived by the pressure-dependent rate constants. Temperature and reaction time dependences of disilane loss and formation of trisilane were well represented by the kinetic simulation. Comparison between the experimental results and the kinetic simulation results suggested that about 70% of consumed disilane was converted to trisilane, which was observed as one of the main reaction products under the present experimental conditions.

Introduction

Thermal decomposition of disilane is of fundamental interest and of technological importance in the semiconductor industry. Disilane is considered as an interesting source for thermal chemical vapor deposition (CVD) of epitaxial silicon, because it pyrolyzes at lower temperatures as compared to silane. Potential energy surfaces of disilane decomposition have been theoretically investigated using quantum chemical calculations.^{1–7} Primary decomposition processes during disilane pyrolysis result from molecular elimination of silane or hydrogen to form silylenes. Figure 1 shows the potential energy surface relevant to thermal dissociation of disilane. Relevant elemental reactions are as follows.



Branching ratios for these three reaction pairs are essential for understanding thermal silicon CVD processes. In particular, formation of Si_2H_4 species is important for low-pressure CVD of polysilicon from silanes. Rate constants of thermal decom-

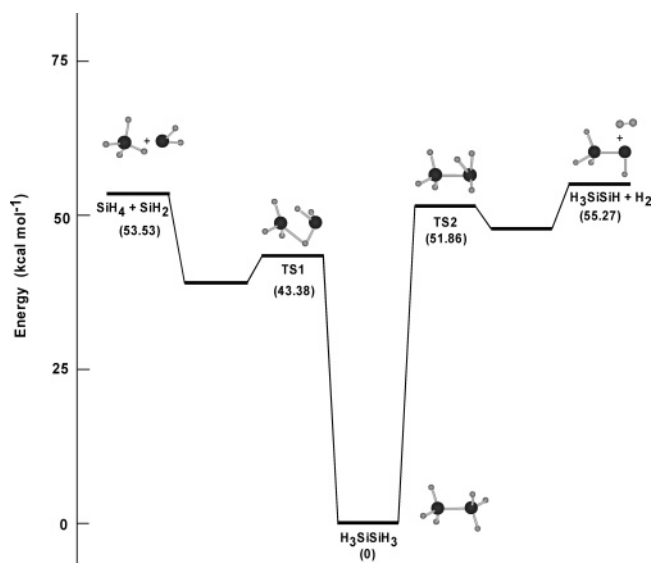


Figure 1. Potential energy surface relevant to thermal dissociation of disilane taken from ref 7. Values in parentheses show the relative energies calculated at the extrapolated QCISD(T) level.

position of disilane have been experimentally measured using static reactors^{8–12} and shock tubes.¹³ Recently, time-of-flight (TOF) mass spectrometry coupled with vacuum ultraviolet single-photon ionization (VUV-SPI) was employed for determination of gas-phase molecules formed following thermal decomposition of disilane.^{5,14,15} Using this method, Si_nH_m species were effectively detected in the gas phase.^{5,14–19} However, information on branching ratios among reaction processes during thermal decomposition of disilane has been very limited.

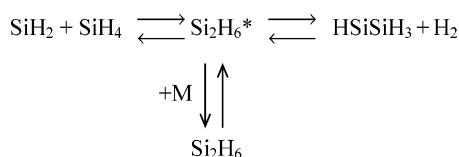
* Corresponding author. Tel.: +81-3-5841-2119. Fax: +81-3-5841-2119. E-mail: tonokura@esc.u-tokyo.ac.jp.

[†] The University of Tokyo.

[‡] Toyohashi University of Technology.

[§] Present address: Environmental Science Center, The University of Tokyo, 7-3-1 Hongo, Bunkyo-ku, Tokyo 113-0033, Japan.

RRKM calculations for thermal decomposition of disilane have been performed by several groups.^{20–26} According to these calculations, reaction R1 dominates, and reaction R2 is believed to be a minor channel because heat of reaction in reaction R1 is lower than that of reaction R2. However, according to results from recent quantum chemical calculations, the difference in reaction enthalpies between reactions R1 and R2 is less than ca. 2 kcal mol⁻¹.^{5–7} It is possible that reaction R2 competes with reaction R1 at high temperatures, and re-examination of branching ratios is required for determination of new values of reaction enthalpy. To the best of our knowledge, no direct experimental information is available for reaction R3. Only one estimated value has been given for reaction R3 by Mick et al.¹³ in their shock tube experiment. To date, there is no experimental information on reactions R-2 and R-3. Girshick et al.²⁷ investigated pressure-dependent rate estimates for the silicon hydride system in their modeling of particle growth during thermal CVD. They found that total pressure had a large effect on the formation of silicon nanoparticles at low pressure while at 1–2 atm particle formation was insensitive to pressure. This finding was attributed to pressure dependence of reactions R-1 and R3. They also showed that temperature-dependent uncertainties existed in rate parameters of chemically activated reactions.²⁸



The rate parameters for these chemically activated channels are only known within roughly an order of magnitude. Recently, Matsumoto et al.⁷ performed RRKM calculations using dual transition state theory treatment for the three reaction pairs. Pressure dependences of various reactions were studied using master equation simulations implementing the two transition state model for microcanonical rate coefficients. Temperature and pressure dependences of the chemical activation reaction R3 and the stabilization reaction R-1 were clarified, and predominance of reactions R-1 and R3 according to temperature and pressure was described.

The present study aimed to understand the primary process in thermal decomposition of disilane. Temperature and time dependences of the reduction of disilane and the formation of trisilane and Si₂H₄ species were measured using TOF mass spectrometry coupled with VUV-SPI. Experimental data were quantitatively interpreted using a gas-phase chemical kinetic model, which included pressure-dependent rate constants of disilane dissociation reactions.

Experimental Section

Experiments were performed using a molecular beam sampling technique combined with TOF mass spectrometry. The methods have been previously described in detail.^{5,14,15} Briefly, the apparatus consisted of a quartz reaction tube incorporated into a source chamber of the molecular beam machine, which was equipped with the Wiley–McLaren-TOF mass spectrometer.²⁹ Reactant gas mixtures were slowly flowed into the quartz reactor (ID = 15 mm) with a sampling hole of 300 μm diameter, placed at the center of the reactor. Products of thermal decomposition were continuously sampled through the pinhole and were collimated by a 1 mm orifice skimmer mounted 4 mm from the pinhole in the reaction tube. The molecular beam

was introduced into the TOF mass spectrometer. For elevated-temperature experiments, Nichrome ribbon was coiled around the reaction tube. Temperature profiles in the reactor were measured using a movable type K thermocouple. Maximum deviation from base temperature in a usable length of 8 cm upstream from the pinhole was ±3%.

Ionization was accomplished by photoionization at 10.5 eV (118 nm). Coherent VUV laser radiation was obtained by frequency tripling in Xe gas.³⁰ A frequency-tripling gas cell coupled with an LiF prism monochromator was sealed at the opposite end of an LiF lens (70 mm focal length at 118 nm) by a fused silica window. A lens with a focal length of 15 cm was used to focus the output (1–8 mJ pulse⁻¹) of a third harmonics of a Nd:YAG laser at 355 nm (Continuum Surelite II) in the cell containing the rare gas. The residual 355 nm laser light was separated from the VUV laser light by a LiF prism monochromator. Dispersed UV light was blocked out by a plate. Spot size of the VUV laser light at the point of molecular beam was about 1 mm. VUV laser light was monitored using a NO-containing photoionization cell. Because a NO molecule has an ionization potential of 9.24 eV, an incident VUV photon at 10.5 eV can ionize the NO molecule. The resultant photocurrent by an ejected electron or ionized NO was monitored to measure the relative intensity of VUV light (~10^{8–10} photon pulse⁻¹).

The ion signal was detected using a two-stage microchannel plate (MCP; Hamamatsu F4655-10). Output of the signal from the MCP was fed to a 500 MHz, 1 GS/s digital oscilloscope (Tektronix TDS 520C), and transferred to a personal computer via a general purpose-interface bus. TOF spectra were accumulated over 1000 laser pulses. Dependence of Si₂H₆⁺ signal versus VUV laser power gave a slope of unity, indicating that ionization resulting from the multiphoton process by the VUV laser light seemed negligible.

Diluted mixtures of disilane (Nippon Sanso, 1.04% Si₂H₆/98.96% He) and trisilane (Takachiho, 1.04% Si₃H₈/98.96% He), and He (Nippon Sanso, >99.9999%) were used without further purifications. The gases were regulated via calibrated mass flow controllers (Kofloc 3650). Gas pressures in the reaction tube were measured with a capacitance manometer (MKS Baratron 622A). Total pressure in the reaction tube was maintained at 20–40 Torr. Initial concentration of disilane was maintained at 1.03 × 10¹⁵ molecule cm⁻³. Reagent concentrations were calculated from total pressure and calibrated flow rates. Residence times (0.01–0.4 s) were controlled by linear flow rates.

Results and Discussion

Single-Photon Ionization Mass Spectra of Disilane and Trisilane. Ionization potentials of disilane and trisilane are 9.67 and 9.31 eV, respectively.^{5,14} Therefore, these species can ionize by vacuum ultraviolet irradiation at 10.5 eV. Figure 2 shows SPI mass spectra of disilane and trisilane at 298 K. No fragmentation signal was observed in the single-photon ionization (SPI) mass spectrum of disilane. Figure 2b shows that fragmentation signals at $m/z = 60–62$ and 90 were observed in the SPI mass spectrum of trisilane. Dependence of ion signals at each m/z on the VUV laser power showed a slope of unity. Hence, ionization resulting from the multiphoton process could be ruled out. Because the appearance potential of Si₂H₄⁺ + SiH₄ + e⁻ in the photoionization of Si₃H₈ is 10.14 eV,¹⁴ production of Si₂H₄⁺ is energetically accessible at 10.5 eV. A fragmentation signal at $m/z = 90$ was observed in photoionization of trisilane. Because the appearance potential of Si₃H₆⁺ + H₂ + e⁻ in the photoionization of trisilane is 9.74 eV,¹⁴ the signal at $m/z = 90$

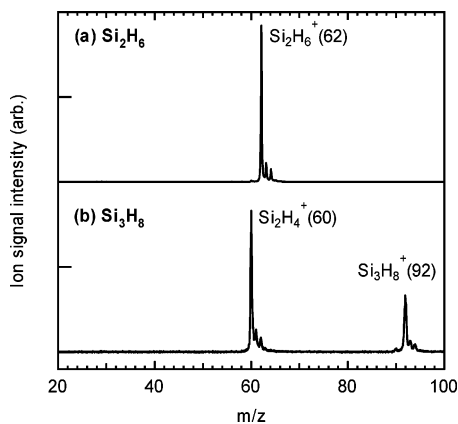


Figure 2. Photoionization mass spectra of (a) disilane and (b) trisilane measured at 10.5 eV (118 nm).

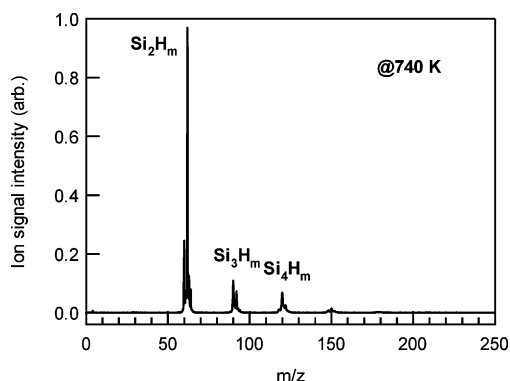


Figure 3. Photoionization mass spectrum during thermal decomposition of disilane at 740 K and at a total pressure of 37.3 Torr. Residence time $t = 0.28$ s.

is caused by this fragmentation process. Therefore, for further analysis, fragmentation signals ($m/z = 60-62, 90$) produced in trisilane photoionization were subtracted from SPI mass spectra for thermal decomposition of disilane.

Unimolecular Decomposition of Disilane. Figure 3 shows the SPI mass spectrum during disilane pyrolysis at 740 K with a total pressure of 40 Torr. Signals at $m/z = 60, 90,$ and 120 resulted from fragmentation of higher $\text{Si}_n\text{H}_{2(n+1)}$ ($n \geq 3$) in the photoionization process. These fragmentation signals did not affect quantification of the $\text{Si}_n\text{H}_{2(n+1)}$ signal. The main component of the ion signal at $m/z = 60$ is the fragmentation signal from trisilane, which is two-thirds of the ion signal at $m/z = 60$. One-third of the ion signal at $m/z = 60$ in Figure 3 is assigned to Si_2H_4 species produced during the thermal decomposition of disilane. The signal assigned to Si_2H_4 at $m/z = 60$ was confirmed by subtracting the contribution from the fragmentation signal of trisilane. Figure 4 shows the corrected spectrum for the fragmentation in the photoionization of trisilane. We also consider the contribution of fragmentation from higher silanes in the mass spectrum. As discussed later, concentration of tetrasilane is 1 order of magnitude smaller than that of trisilane. The upper limit of the contribution of fragmentation at $m/z = 60$ from higher silanes would be 10% under the assumption that the ionization cross section of the $\text{Si}_2\text{H}_4^+ + \text{Si}_2\text{H}_6 + e^-$ process in the photoionization of Si_4H_{10} is the same order of magnitude as that of $\text{Si}_2\text{H}_4^+ + \text{SiH}_4 + e^-$ in the photoionization of Si_3H_8 . The ion signal at $m/z = 90$ is a signal of Si_3H_6 species and/or a fragmentation signal in the photoionization of Si_4H_{10} . Observations of $\text{Si}_2\text{H}_m, \text{Si}_3\text{H}_m,$ and

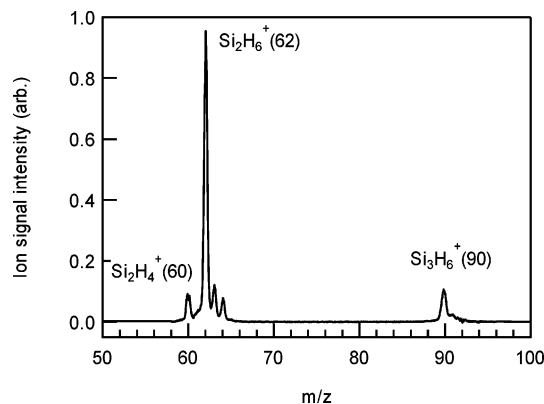
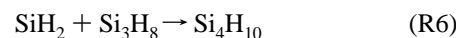
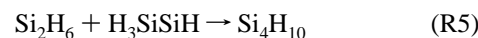
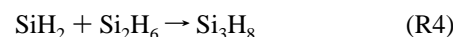


Figure 4. Photoionization mass spectrum corrected for the contribution of fragmentation of trisilane according to the method described in the text.

Si_4H_m species in Figure 3 were consistent with a previously proposed thermal decomposition mechanism of disilane.^{5,31,32}



Reactions R1 and R2 are primary processes of unimolecular dissociation of disilane. Reactions R4, R5, and R6 are sequential reactions leading to a higher cluster formation. As shown in Figure 3, a contribution of the sequential reaction to produce higher Si_n species was small at a reaction temperature < 740 K. Therefore, to understand the primary process of unimolecular dissociation of disilane, we used a reaction temperature below 740 K in the present study.

Time profiles of Si_2H_6 ($m/z = 62$), Si_3H_8 ($m/z = 92$), and Si_2H_4 ($m/z = 60$) as a function of reaction time were measured at a fixed temperature. Figure 5 shows a typical example measured at 720 K and 36.5 Torr. Absolute concentrations of disilane and trisilane were derived from the calibration curve. On the other hand, quantification of Si_2H_4 was experimentally difficult due to the absence of a standard sample, and the absence of photoionization cross-section data. Si_2H_6 intensity decreased by promotion of unimolecular decomposition as a function of reaction time, while productions of trisilane and Si_2H_4 species were observed. Figure 6 shows reaction temperature dependence of disilane reduction and productions of Si_3H_8 and Si_2H_4 at a reaction time $t = 0.27$ s and $P = 35$ Torr. Promotion of the unimolecular decomposition of disilane and productions of trisilane and Si_2H_4 species were clearly observed as a function of reaction temperature.

Comparison with Model Calculations. Kinetic modeling was carried out using CHEMKIN 4 program packages with a set of reactions to simulate gas-phase chemical kinetics of thermal decomposition of Si_2H_6 at each experimental temperature. On the basis of the chemical kinetic model proposed by Swihart and Girshick (SG),³¹ we constructed a chemical reaction model that had a total of 48 gas-phase reactions and 28 surface reactions, involving 30 chemical species up to 5 silicon atoms (the modified SG (MSG1) model). Gas and surface reactions were incorporated into the model using the CRESLAF program³² from the CHEMKIN family of codes. Plug flow condition was

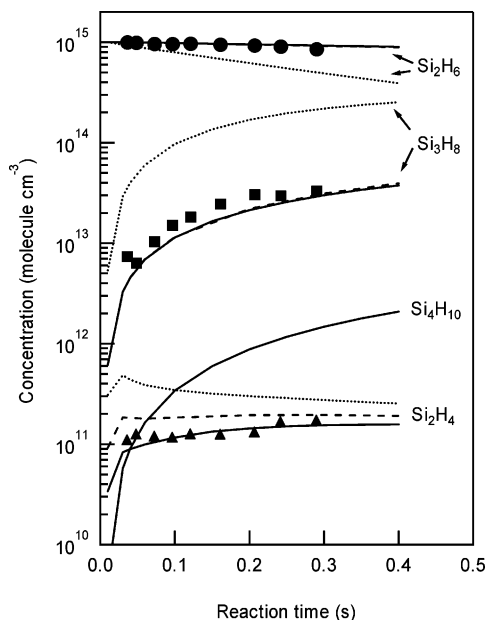


Figure 5. Concentration profiles of Si_2H_6 (●), Si_3H_8 (■), and Si_2H_4 (▲) as a function of reaction time. Curves are modeling results, the MSG1 model (solid curves), the MSG2 model (broken curves) in which rate parameters of reactions R2 and R-2 are those of the NSG model, and the NSG model (dotted curves). Experimental results of Si_2H_4 are offset to the simulation value (1.16×10^{11} molecule cm^{-3}) at $t = 0.1$ s. Concentration profile of Si_4H_{10} calculated by MSG1 model is also shown. Reaction temperature $T = 720$ K. $P = 36.5$ Torr.

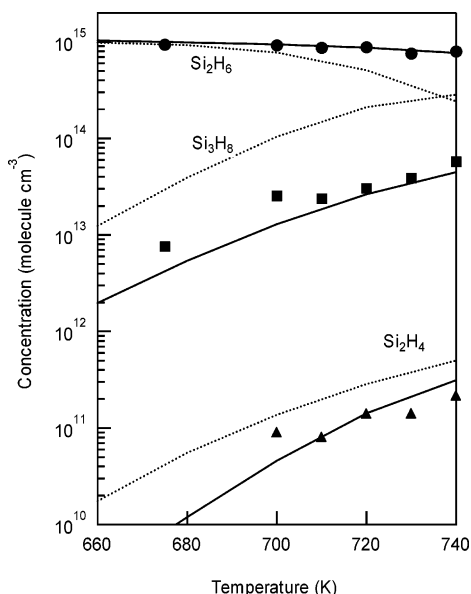


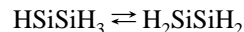
Figure 6. Concentration profiles of Si_2H_6 (●), Si_3H_8 (■), and Si_2H_4 (▲) as a function of reaction temperature. Curves are modeling results, the MSG1 model (solid curves), and the NSG model (dotted curves). Experimental results of Si_2H_4 are offset to the simulation value (1.40×10^{11} molecule cm^{-3}) at $T = 720$ K. Reaction time $t = 0.27$ s. $P = 35$ Torr.

assumed in this simulation. The gas-phase rate constants used in our model are almost the same as those proposed by Girshick et al.²⁷ In our model, reaction 11 in Table 1 of ref 27 ($\text{SiH}_2 + \text{M} = \text{Si} + \text{H}_2 + \text{M}$) is deleted and disilane dissociation rate constants (reactions 2, 3, and 7 in Table 1 of ref 27) are replaced by the pressure-dependent rate constants proposed by Matsuoto et al.,⁷ which are listed in Table 1. For example, at $T = 720$ K and $P = 36.5$ Torr, the rate constant for (R1) is $9.82 \times 10^{-2} \text{ s}^{-1}$ and that for (R2) is $1.03 \times 10^{-3} \text{ s}^{-1}$. The surface-

phase rate constants used in our model are almost the same as those proposed by Ho et al.³³ In our model, a hydrogen desorption reaction rate constant ($2\text{SiH}(\text{S}) = 2\text{Si}(\text{S}) + \text{H}_2$) is replaced by that proposed by Sinniah et al.³⁴ ($A = 2.2 \times 10^{11}$, $E_a = 43\,000$). Temperature-dependent sticking coefficients for SiH_4 , Si_2H_6 , and Si_3H_8 and the sticking coefficient for Si_2H_4 (unity) are the same as those proposed by Ho et al. Full reaction rate parameters used in this study are listed in Supporting Information tables.

As depicted in Figure 1, the transition states for the dissociation of disilane are lower in energy than the corresponding separated products. As discussed in our previous paper, ref 7, the bottleneck for the dissociation varies with temperature. Disilane dissociation rate constants in Table 1 correspond to those in the 500–1000 K temperature range and are in the falloff region, not in the high-pressure-limit. In the falloff region, the distribution functions are nonequilibrium (non-Boltzmann distributions) and microcanonical rate constants are averaged over the nonequilibrium distribution functions to obtain canonical rate constants. By these reasons, activation energy, E_a , in disilane dissociation rate constants of Table 1 do not coincide with the values in Figure 1.

Comparisons between experimental data and simulation results using the MSG1 model and normal SG (NSG) model are given in Figures 5 and 6. Tonokura et al.⁵ qualitatively compared the concentration profiles of Si_mH_m species between experimental and simulation results. They simulated the concentration profiles using the NSG model, and only concentration profiles of disilane have been quantitatively compared. As shown in Figures 5 and 6, concentration profiles of disilane using present modeling results have improved from the NSG model and are in good agreement with experimental results. In the present study, quantitative comparison of trisilane concentrations between experimental and modeling results was also available. Concentration profiles of trisilane between experimental and the present modeling results reasonably agreed, and the experimental results showed higher concentrations than in the modeling results with a maximum deviation of ca. 50%. The concentration profile of tetrasilane calculated by MSG1 model is also shown in Figure 5. The concentration of tetrasilane is 1 order of magnitude smaller than that of trisilane. Although tetrasilane production was minimized under the present experimental conditions, the fragmentation signal from photoionization of higher silanes could not be completely ruled out. This could be one of the reasons for the higher estimation of trisilane concentration in the present study. We also compared experimental results of Si_2H_4 with simulation results of Si_2H_4 species by the MSG1 model. Isomerization between silylsilylene (HSiSiH_3) and silene (H_2SiSiH_2) was definitely involved in the modeling.



The isomerization barrier of HSiSiH_3 to H_2SiSiH_2 was $7.0 \text{ kcal mol}^{-1}$. The main pathway of reduction of HSiSiH_3 involves isomerization to H_2SiSiH_2 under the present experimental conditions.¹⁴ Kinetic simulation results suggested that the concentration of H_2SiSiH_2 was roughly 2 orders of magnitude higher than that of HSiSiH_3 . Hence, the observed Si_2H_4 species in the experiment would mainly represent H_2SiSiH_2 . Simulation results of Si_2H_4 species in Figures 5 and 6 show the concentration of H_2SiSiH_2 . As discussed above, the signal assigned to Si_2H_4 at $m/z = 60$ was obtained by subtracting the contribution from the fragmentation signal. There are no data on the photoionization cross section and no standard sample of Si_2H_4 .

TABLE 1: Disilane Dissociation Rate Constants in Our Model^a

reaction	<i>P</i> = 36.5 Torr (Figure 5)			<i>P</i> = 35.0 Torr (Figure 6)		
	<i>A</i> (cm ³ mol, s)	β	<i>E_a</i> (cal/mol)	<i>A</i> (cm ³ mol, s)	β	<i>E_a</i> (cal/mol)
Si ₂ H ₆ (+M) = SiH ₂ + SiH ₄ (+M)	5.27E+12	0.0	45765.0	5.02E+12	0.0	45724.7
(reverse reaction)	1.32E+11	0.0	-6897.7	1.26E+11	0.0	-6926.3
Si ₂ H ₆ (+M) = H ₃ SiSiH + H ₂ (+M)	4.81E+10	0.0	45549.1	4.58E+10	0.0	45514.0
(reverse reaction)	1.31E+08	0.0	-11200.6	1.23E+08	0.0	-11235.9
SiH ₂ + SiH ₄ (+M) = H ₃ SiSiH + H ₂ (+M)	9.55E+12	0.0	2140.6	9.44E+12	0.0	2116.3
(reverse reaction)	1.20E+12	0.0	-2041.6	1.19E+12	0.0	-2055.9

^a Forward and reverse rate constants are expressed in the form $k_f = AT^\beta \exp(-E_a/RT)$. Rate parameters are given in the units of molecule, cm, s, cal, and K.

Therefore, we attempted to qualitatively analyze Si₂H₄. Figure 5 shows that experimental results of Si₂H₄ are offset to the simulation value (1.16×10^{11} molecule cm⁻³) at $t = 0.1$ s. The NSG model results show a profile with rise and decay, while experimental results and the MSG1 model results show an increase in Si₂H₄ concentration. The concentration profile of Si₂H₄ by the MSG1 model is in good agreement with experimental results. Concentrations of Si₂H₆, Si₃H₈, Si₂H₄, Si₄H₁₀, and SiH₄ and branching ratios of SiH₄ to Si₃H₈ at $T = 720$ K and $P = 36.5$ Torr as a function of reaction time measured in the present experiments and predicted by the MSG1 model are shown in Supporting Information tables.

In Figure 6, experimental results of Si₂H₄ at $T = 720$ K are offset to the simulation value (1.40×10^{11} molecule cm⁻³). The concentration profile of Si₂H₄ qualitatively agrees with the present simulation results. In the present simulation, the production of Si₂H₄ is not affected by reactions R3 and R-3.

To quantitatively evaluate the production pathway of Si₂H₄, the concentration profiles of disilane, trisilane, and Si₂H₄ species are simulated by another modified SG (MSG2) model in which the rate parameters of reactions R2 and R-2 are those of the NSG model, while the rate parameters of reactions R1, R-1, R3, and R-3 are those of Table.1. As shown in Figure 5, concentration profiles of disilane and trisilane by the MSG2 model are almost the same as those by the MSG1 model. Concentration of Si₂H₄ by the MSG2 model increases as compared to those by the MSG1 model. For example, at reaction time = 0.1 s, the concentration of Si₂H₄ by the MSG2 model is 1.83×10^{11} molecule cm⁻³ as compared to 1.16×10^{11} molecule cm⁻³ by the MSG1 model. This variation is attributed to reactions R2 and R-2. It indicates that in the present simulation, disilane dissociation reaction Si₂H₆ → H₂ + H₃-SiSiH, (R2), is one of the main production pathways of Si₂H₄. On the other hand, the concentration profile of Si₂H₄ by the MSG2 model decreases as compared to those by the NSG model. For example, at reaction time = 0.1 s, the concentration of Si₂H₄ is 3.44×10^{11} molecule cm⁻³ by NSG model. The variation is mainly attributed to the reaction of SiH₂ + Si₂H₆ = SiH₄ + HSiSiH₃. This reaction is one of the relevant reactions in the thermal decomposition of trisilane, which are not studied in this paper. To further discuss the production pathway of Si₂H₄, evaluation of the relevant rate constants of the thermal decomposition of trisilane is needed.

In Figure 6, the concentration of Si₂H₆ at $T = 720$ K is 8.75×10^{14} molecule cm⁻³, which corresponds to a reaction ratio $1 - \{[Si_2H_6]/[Si_2H_6]_0\}$ of 0.15. This value is in excellent agreement with the simulation value of 0.16. Production ratio $[Si_3H_8]/[Si_2H_6]_0$ at $T = 720$ K is estimated to be 0.029. This value is also in excellent agreement with the simulation value of 0.025. Trisilane and silane are the main gas-phase products of the thermal decomposition of disilane. The main reaction pathway producing trisilane is reaction R4, SiH₂ + Si₂H₆ → Si₃H₈, in which SiH₂ is produced from thermal dissociation of disilane,

(R1). Two disilane molecules are consumed by the production of trisilane. From the reaction ratio and the production ratio, it is estimated that ca. 70% of consumed disilane become trisilane at $T = 720$ K, $t = 0.27$ s, and $P = 35$ Torr. Another pathway for consumption of SiH₂ produced in reaction R1 is a heterogeneous reaction occurring on the reaction tube surface. Although simulation results suggested that the concentration of silane was 1.5 times higher than that of tridisilane at $T = 720$ K, $t = 0.27$ s, and $P = 35$ Torr, the concentration of silane was not experimentally determined due to a higher ionization potential (11.0 eV) than VUV photon energy (10.5 eV). The main production pathway of silane is reaction R1, Si₂H₆ → SiH₄ + SiH₂.

Conclusions

The thermal decomposition mechanism of disilane was studied by comparison between experimental and kinetic simulation results. Experimental concentration profiles of disilane and trisilane quantitatively agreed with kinetic simulation data, which incorporate pressure-dependent rate constants resulting from disilane decomposition. The branching ratio for (R1)/(R2) can be derived by the pressure-dependent rate constants, for example, at $T = 720$ K and $P = 36.5$ Torr, the (R1)/(R2) is 95.3. The concentration of Si₂H₄ species was estimated to be more than 10^{10} molecule cm⁻³ under the present experimental conditions ($T < 740$ K and $P < 40$ Torr). The production of Si₂H₄ is not affected by reaction of SiH₂ + SiH₄ → H₃SiSiH + H₂ in the present conditions. Under the present experimental conditions, one of the main production pathways of Si₂H₄ species is Si₂H₆ → Si₂H₄ + H₂ reaction. The main production pathway of trisilane is SiH₂ + Si₂H₆ → Si₃H₈ reaction.

Acknowledgment. This study was supported by the Ministry of Education, Culture, Sports, Science, and Technology of Japan Grant for the 21st Century COE Program "Center of Excellence for Human-Friendly Materials on Chemistry".

Supporting Information Available: Full reaction parameters in thermal decomposition of disilane and data on the time profiles of Si_{*n*}H_{*m*} species shown in Figure 5. This material is available free of charge via the Internet at <http://pubs.acs.org>.

References and Notes

- Ignacio, E. W.; Schlegel, H. B. *J. Phys. Chem.* **1992**, *96*, 1758.
- Sakai, S.; Nakamura, M. *J. Phys. Chem.* **1993**, *97*, 4960.
- Becerra, R.; Frey, H. M.; Mason, B. P.; Walsh, R.; Gordon, M. S. *J. Chem. Soc., Faraday Trans.* **1995**, *91*, 2723.
- Swihart, M. T.; Carr, R. W. *J. Phys. Chem. A* **1997**, *101*, 7434.
- Tonokura, K.; Murasaki, T.; Koshi, M. *J. Phys. Chem. B* **2002**, *106*, 555.
- Hu, S.-W.; Wabg, Y.; Wang, X.-Y.; Chu, T.-W.; Liu, X.-Q. *J. Phys. Chem. A* **2003**, *107*, 2954.

- (7) Matsumoto, K.; Klippenstein, S. J.; Tonokura, K.; Koshi, M. *J. Phys. Chem. A* **2005**, *109*, 4911.
- (8) Bowrey, M.; Purnell, J. H. *Proc. R. Soc. London, Ser. A* **1971**, *321*, 341.
- (9) Olbrich, G.; Potzinger, P.; Reimann, B.; Walsh, R. *Organometallics* **1984**, *3*, 1267.
- (10) Martin, J. G.; Ring, M. A.; O'Neal, H. E. *Int. J. Chem. Kinet.* **1987**, *19*, 715.
- (11) Martin, J. G.; O'Neal, H. E.; Ring, M. A. *Int. J. Chem. Kinet.* **1990**, *22*, 613.
- (12) Dzarnoski, J.; Rickborn, S. F.; O'Neal, H. E.; Ring, M. A. *Organometallics* **1982**, *1*, 1217.
- (13) Mick, H. J.; Markus, M. W.; Roth, P.; Smirnov, V. N. *Ber. Bunsen. Phys. Chem.* **1995**, *99*, 880.
- (14) Tonokura, K.; Murasaki, T.; Koshi, M. *Chem. Phys. Lett.* **2000**, *319*, 507.
- (15) Tonokura, K.; Koshi, M. *Curr. Opin. Solid State Mater. Sci.* **2002**, *6*, 479.
- (16) Tada, N.; Tonokura, K.; Matsumoto, K.; Koshi, M.; Miyoshi, A.; Matsui, H. *J. Phys. Chem. A* **1999**, *103*, 322.
- (17) Nakajima, Y.; Tonokura, K.; Sugimoto, K.; Koshi, M. *Int. J. Chem. Kinet.* **2001**, *33*, 136.
- (18) Chambreau, S. D.; Zhang, J. S. *Chem. Phys. Lett.* **2001**, *343*, 482.
- (19) Chambreau, S. D.; Wang, L.; Zhang, J. S. *J. Phys. Chem. A* **2002**, *106*, 5081.
- (20) Frey, H. M.; Walsh, R.; Watts, I. M. *J. Chem. Soc., Chem. Commun.* **1986**, 1189.
- (21) (a) Roenigk, K. F.; Jensen, K. F.; Carr, R. W. *J. Phys. Chem.* **1987**, *91*, 5726. (b) Roenigk, K. F.; Jensen, K. F.; Carr, R. W. *J. Phys. Chem.* **1987**, *91*, 5732.
- (22) Moffat, H. K.; Jensen, K. F.; Carr, R. W. *J. Phys. Chem.* **1992**, *96*, 7683.
- (23) Moffat, H. K.; Jensen, K. F.; Carr, R. W. *J. Phys. Chem.* **1992**, *96*, 7695.
- (24) Mick, H. J.; Roth, P.; Sminrov, V. N. *Kinet. Catal.* **1996**, *37*, 1.
- (25) Smirnov, V. N. *Kinet. Catal.* **1997**, *38*, 309.
- (26) Swihart, M. T.; Carr, R. W. *J. Phys. Chem. A* **1998**, *102*, 1542.
- (27) Girshick, S. L.; Swihart, M. T.; Suh, S. M.; Mahajan, M. R.; Nijhawan, S. *J. Electrochem. Soc.* **2000**, *147*, 2303.
- (28) Nijhawan, S.; McMurry, P. H.; Swihart, M. T.; Suh, S. M.; Girshick, S. L.; Campbell, S. A.; Brockmann, J. E. *J. Aerosol Sci.* **2003**, *34*, 691.
- (29) Wiley, W. C.; McLaren, I. H. *Rev. Sci. Instrum.* **1955**, *26*, 1150.
- (30) Hilbig, R.; Wallenstein, R. *IEEE J. Quantum Electron.* **1981**, *QE-17*, 1566.
- (31) Swihart, M. T.; Girshick, S. L. *J. Phys. Chem. B* **1999**, *103*, 64.
- (32) Coltrin, M. E.; Moffatt, K.; Kee, R. J.; Rupley, F. M. *Creslaf (Version 4.0): A Fortran Program for Modeling Laminar, Chemically Reacting Boundary-Layer Flowing Cylindrical or Planar Channels*; Sandia National Laboratories Report, SAND93-0478, 1993.
- (33) Ho, P.; Coltrin, M. E.; Breiland, W. G. *J. Phys. Chem.* **1994**, *98*, 10138.
- (34) Sinniah, K.; Sherman, M. G.; Lewis, L. B.; Weinberg, W. H.; Yates, J. T., Jr.; Janda, K. C. *J. Chem. Phys.* **1990**, *92*, 5700.